molecular pharmaceutics

COMMUNICATION

pubs.acs.org/molecularpharmaceutics

Hybrid Nanocrystals: Achieving Concurrent Therapeutic and Bioimaging Functionalities toward Solid Tumors

Rongsheng Zhao,[†] Christin P. Hollis,[†] Hua Zhang,[†] Lili Sun,[†] Richard A. Gemeinhart,[‡] and Tonglei Li[*,†]

[†]Pharmaceutical Sciences, University of Kentucky, Lexington, Kentucky 40536, United States

[‡]Biopharmaceutical Sciences, Bioengineering, and Ophthalmology and Visual Sciences, University of Illinois, Chicago, Illinois 60612, United States

ABSTRACT: Bioimaging and therapeutic agents accumulated in ectopic tumors following intravenous administration of hybrid nanocrystals to tumor-bearing mice. Solid, nanosized paclitaxel crystals physically incorporated fluorescent molecules throughout the crystal lattice and retained fluorescent properties in the solid state. Hybrid nanocrystals were significantly localized in solid tumors and remained in the tumor for several days. An anticancer effect is expected of these hybrid nanocrystals.

KEYWORDS: nanocrystals, anticancer, bioimaging, theranostics, paclitaxel

INTRODUCTION

Antineoplastic chemotherapy remains a cornerstone of cancer treatment. Delivery of chemotherapeutic agents to cancer patients nonetheless faces two major hurdles. The first hurdle is the omnipresent cytotoxicity of anticancer compounds that also damage healthy cells, presenting a grave danger to vital organs and the immune system. The second hurdle stems from extremely poor water solubility of many antineoplastic agents. A common practice of drug delivery is taking obvious, ostensibly simple routes to solubilize drug substances prior to administration, including solvent-based, and surfactant, polymer, or lipid encapsulating systems.[1,2] Such designs become overly complicated when they also attempt to address the first challenge by forming nanosized particles taking advantage of the enhanced permeability and retention (EPR) effect.[3] EPR is a hallmark of targeted cancer drug delivery, in which the vasculature in a tumor mass is much more "leaky" than that in healthy tissues, allowing the circulating drug carriers to enter the tumor and get trapped because of the tumor's poorly developed lymphatic system. Typically, these approaches limit drug loading, raise concerns of system integrity and physical stability, and, in the end, render many of these efforts futile.

Suspensions of drug nanocrystals have recently been explored for delivering anticancer drugs.[4−6] There has been significant effort with a few products reaching clinical trials and the market.[7,8] Administering a poorly soluble drug directly as nanocrystals circumvents the need of solubilization and avoids subsequent caveats. Preparation of nanocrystals can be done by either a top-down approach, such as milling, or a bottom-up approach of controlled crystal growth.[9,10] Nevertheless, it appears exceedingly difficult to securely integrate functional chemicals, such as bioimaging agents, into drug nanocrystals, which are constantly dissolving *in vivo*, albeit slowly for poorly soluble drugs.

To construct multicomponent and thereby multifunctional nanocrystals, we have resorted to a well-known phenomenon in solid-state chemistry: guest inclusions. It has been observed that guest molecules can be embedded or grown into the lattice of a crystal host as defects—the amount of guests is typically minute—rendering significant changes to specific properties of the host, such as optical appearance, mechanical durability, and electronic conductivity. Examples are abundant, including both natural (e.g., colored diamonds) and synthetic (e.g., alloys and p- and n-type semiconductors). We are particularly inspired by the studies of dyeing crystals wherein organic colorants are embedded in an organic crystal.[11] The essence of our idea of delivering poorly soluble drugs is thereby to integrate functional guest substances in the crystal lattice of a therapeutic compound. By producing such a hybrid system in nanosized crystals, concurrent tumor targeting and imaging become feasible. Herein, we report a recent study growing and testing paclitaxel nanocrystals that integrate fluorescent molecules. Although fluorescent probes are gaining acceptance in clinical medicine,[12,13] fluorescent probes may not be appropriate for all human imaging applications. This proof-of-concept study may open the door for incorporating other types of imaging agents for clinical application (such as radionuclides).

EXPERIMENTAL SECTION

Materials. Paclitaxel (>99.5%, USP30) was purchased from 21CECPharm (East Sussex, United Kingdom); FPR-749 fluorophore (maximum excitation wavelength, λ_{ex} = 749 nm; maximum emission, λ_{em} = 782 nm) was from Akina (West Lafayette, IN); fluorescein (λ_{ex} = 494 nm, λ_{em} = 521 nm) and Rhodamine B (λ_{ex} = 530 nm, λ_{em} = 590 nm) were from Sigma (St. Louis, MO). Ethanol (HPLC grade), acetonitrile (HPLC grade), and DMSO (dimethyl sulfoxide, ACS grade) were purchased from Fisher Scientific (Pittsburgh, PA). All chemicals and solvents were utilized without further purification. Deionized water (by Milli-Q, filtered through 0.2 μm membrane) was used for all experiments. Whatman Nuclepore polycarbonate track-etched membranes used for filtration were purchased from Fisher Scientific (Pittsburgh, PA).

Preparation of Nanocrystals. Pure and hybrid paclitaxel nanocrystals were produced by using an antisolvent method.

Received: March 28, 2011
Revised: July 27, 2011
Accepted: August 3, 2011
Published: August 03, 2011

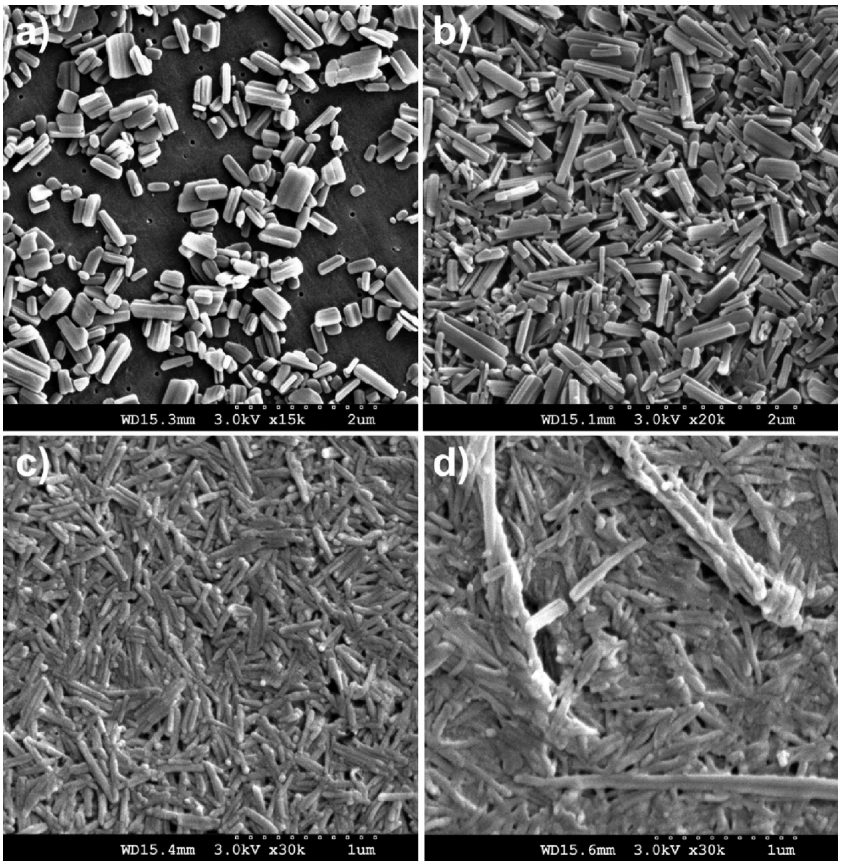

Figure 1. Crystals are formed from the nanoprecipitation process. Scanning electron micrographs of nanocrystal samples, paclitaxel (a), hybrid paclitaxel/FPR-749 (b), paclitaxel/fluorescein (c), and paclitaxel/Rhodamine B (d) have regular needle-like shape.

In a typical experiment, 1 mL of 5 mg/mL of paclitaxel in ethanol was added to 20 mL of deionized water. The mixture was stirred at 1,000 rpm with stirrer shaft in a round-bottom flask immerged in a sonication bath (F20D, Fisher Scientific). The stirring speed was adjusted subsequently in order to minimize bubbles formed and to promote uniform nucleation. After crystallization, the solution was filtered with a 50 nm polycarbonate filter paper and the retentate was air-dried, resuspended in water, and underwent additional filtration−resuspension cycles. To make hybrid nanocrystals, the same procedure was used with the exception of dissolving 5 mg/mL dye in the deionized water prior to the crystallization process.

Analysis of Nanocrystals. SEM images were obtained using a Hitachi SEM 4300 at an accelerating voltage of 3 kV. Prior to visualization, using a sputter coater, samples were coated with conductive layers of gold palladium (Au/Pd) for 1 min with a current of 20 mA, resulting in an approximately 15 nm thick coating. In addition to SEM analysis, particle size and zeta potential were measured in distilled deionized water using a Malvern Zetasizer (Nano-ZS). As a preliminary assessment of crystallinity, X-ray power diffraction was collected on a powder X-ray diffractometer (Multiplex, Rigaku) with Cu Kα radiation (40 kV, 44 mA). Scans were obtained from 5 to 40° with step size of 0.04° and scan rate of 0.5°/min.

Quantification of paclitaxel was conducted by high pressure liquid chromatography (HPLC, Waters Breeze) with a Waters Symmetry C18 5 μm column (4.6 × 150 mm); it was analyzed by a UV detector (Waters 2487 dual λ absorbance detector) at 227 nm with a mobile phase of ethanol/acetonitrile (50:50) pumped at a rate of 1.5 mL/min (Waters 1525 binary pump).

Measurement of the fluorophores was by fluorescence plate readers. Standard solutions of FR-749 fluorophore with concentrations ranging from 39 ng/mL to 1.25 μg/mL were prepared in DMSO and measured at excitation and emission wavelengths of 766 and 799 nm, respectively, by SpectraMax M5 (Molecular Devices). Fluorescein and Rhodamine B were analyzed by similar methods.

Cell Culture. The MCF-7 breast cancer cells were cultured in DMEM (Dulbecco's modified Eagle's medium, Hyclone) with 10% fetal bovine serum (Hyclone) and 1% penicillin/streptomycin (Hyclone). Trypsin−EDTA (ethylenediaminetetraacetic acid, Mediatech) was used to dissociate cells from the dish. All the cell culture reagents were purchased from Fisher Scientific (Pittsburgh, PA). Cells were cultured at 37 °C in a humidified atmosphere with 5% CO_2.

Animal Study. The study was conducted under a protocol approved for using nude mice by the University's Institutional Animal Care and Use Committee (IACUC) to study the treatment efficacy and bioimaging of drug nanocrystals. Female nude outbred mice (Tac:Cr: (NCr)-Foxn1 Nu) were obtained from Taconic at 3−4 weeks of age (14.5−20 g). To minimize discomfort to the animals, all proposed experimental procedures were performed under general anesthesia by isoflurane inhalation (approximately 20 s). Seven days after arrival, one 17β-estradiol pellet (1.7 mg, 60-day release; Innovative Research , Inc.) was implanted surgically, under the skin, between the ears of each mouse.

Subsequently, two days later, 5×10^6 MCF-7 cells (100 μL) were inoculated subcutaneously to each side of the flank by using 25−30 gauge needles. Mice were then returned immediately to their housing and observed until they were responsive. Animals were monitored daily for their weight, body condition scoring (BCS), and general tumor status. Any moribund animals would be euthanized. Once the tumor was palpable (i.e., at least having tumor size of 200 mm^3), mice were randomly assigned to treatment or control group. Mice were restrained during the tail vein injection. Each mouse, except for the control group, was injected with formulation dose of 20 mg/kg paclitaxel.

For the saline injection, a total of 100 μL of 0.9% sodium chloride (Irrigation, USP grade, Aqualite System, Hospira Inc., Lake Forest, IL) was injected. For the paclitaxel formulation, 3 mg/mL paclitaxel was prepared by diluting 300 μL of 30 mg/mL of paclitaxel in Cremophore EL/ethanol (50:50) solution with 2700 μL of saline (0.9% sodium chloride). The suspension was sonicated after mixing and immediately before injection to the animal to ensure that there was no large precipitate formed. For the pure and hybrid paclitaxel nanocrystals, nanocrystals were concentrated by filtering (with 50 nm Nuclepore filter) and resuspension in deionized water by sonication. The concentration of the formulation was approximately 3 mg/mL. Depending on the body weight of the mouse, the volume of injection varied, but it did not exceed 200 μL, the recommended maximum injection volume for mice. All animals were euthanized 7 days after the treatment day by CO_2 inhalation, followed by cervical dislocation.

***In Vivo* Imaging.** *In vivo* optical imaging was obtained by using the Caliper IVIS Spectrum. The excitation and emission wavelengths used to visualize FPR-749 fluorophore were 740 and 780 nm, respectively. At these wavelengths, the mice injected with Rhodamine B exhibited minimal background fluorescence. To visualize one with Rhodamine B, the excitation and emission wavelengths were 535 and 580 nm, respectively. For comparison, all imaging parameters, including exposure time, *F*-stop (2), and binning (medium), were maintained throughout the 7-day experiment.

RESULTS AND DISCUSSION

Pure and hybrid paclitaxel nanocrystals were prepared. Several dye substances were used as the guest, including fluorescein, Rhodamine B, and FPR-749. The average sizes, estimated from the SEM images (Figure 1a−d), were 350 and 700 nm in length, respectively, of pure and hybrid paclitaxel nanocrystals while light scattering of paclitaxel nanocrystals suggested particles were 438.5 ± 8.3 nm with polydispersity index of 0.242 ± 0.007 in good agreement with SEM observations. Zeta potential of paclitaxel nanocrystals (pure and hybrid) ranged from −15 to −22 mV. The nanocrystal samples were physically stable, and no drastic change in particle size or shape was seen over six months in solution (verified by SEM). The stability was likely due to the negative surface potential, and we plan to study the stability of these particles in more detail. Although the particles are stable for this period in water as individual particles, further investigation is necessary to understand the physical stability of the particles during the long-term storage.

The regular, elongated prismatic morphology of the prepared nanoparticles suggests the crystalline nature of the solid samples as the same morphology was observed on larger, microsized drug crystals. In addition, powder X-ray diffraction patterns (Figure 2) exhibited sharp bands typical of crystalline substances. The

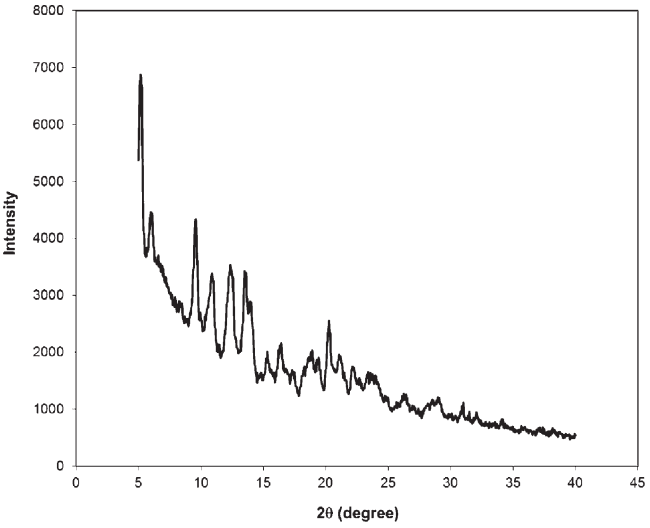

Figure 2. X-ray diffraction pattern of paclitaxel nanocrystals.

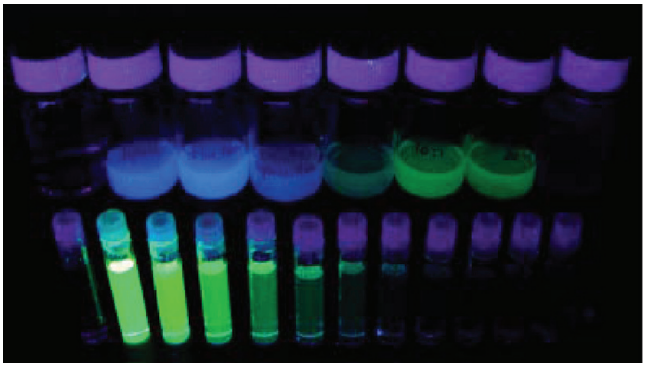

Figure 3. Hybrid paclitaxel nanocrystals with fluorescein under UV light. Back row (left to right): pure solvent, 0.015, 0.028, 0.022, 0.25, 0.83, and 0.86% dye in hybrid nanocrystals, and pure paclitaxel nanocrystals. Front row (left to right): samples of pure dye solutions to pure solvent, 4, 2, 1, 0.5, 0.25, 0.125, 0.0625, 0.031, 0.008, 0.002, 0.0005 μg/mL.

diffraction pattern of paclitaxel nanocrystals matches that of paclitaxel dihydrate.[14]

The amount of dye molecules in hybrid paclitaxel nanocrystals was analyzed spectroscopically. The weight/weight ratios of fluorescein, Rhodamine B, and FPR-749 were measured and results distributed widely; the highest values of prepared samples were 0.86%, 1.26%, and 0.79%, respectively. Note that the hybrid nanocrystals were washed several times by a filtration−rinse−suspension cycle to minimize loosely bound dye on crystal surfaces. To confirm bioimaging capability, paclitaxel/fluorescein hybrid nanocrystals were dispersed in water and irradiated under a UV light (emission peak at 365 nm). The hybrid nanocrystal samples clearly showed fluorescence emission (Figure 3). Because drug solubility was low (*ca.* 0.2 μg/mL), there was estimated to be less than 0.002 μg/mL free fluorescein molecules released into solution when the fluorescein was entrapped at a 0.86% entrapment ratio (Figure 3, back row, second from right). For such a small amount, no fluorescence could be visibly observed from the freely dissolved dye molecules as suggested by the pure dye solutions (Figure 3, front row, second from right). The fluorescence of the hybrid nanocrystal samples was thereby

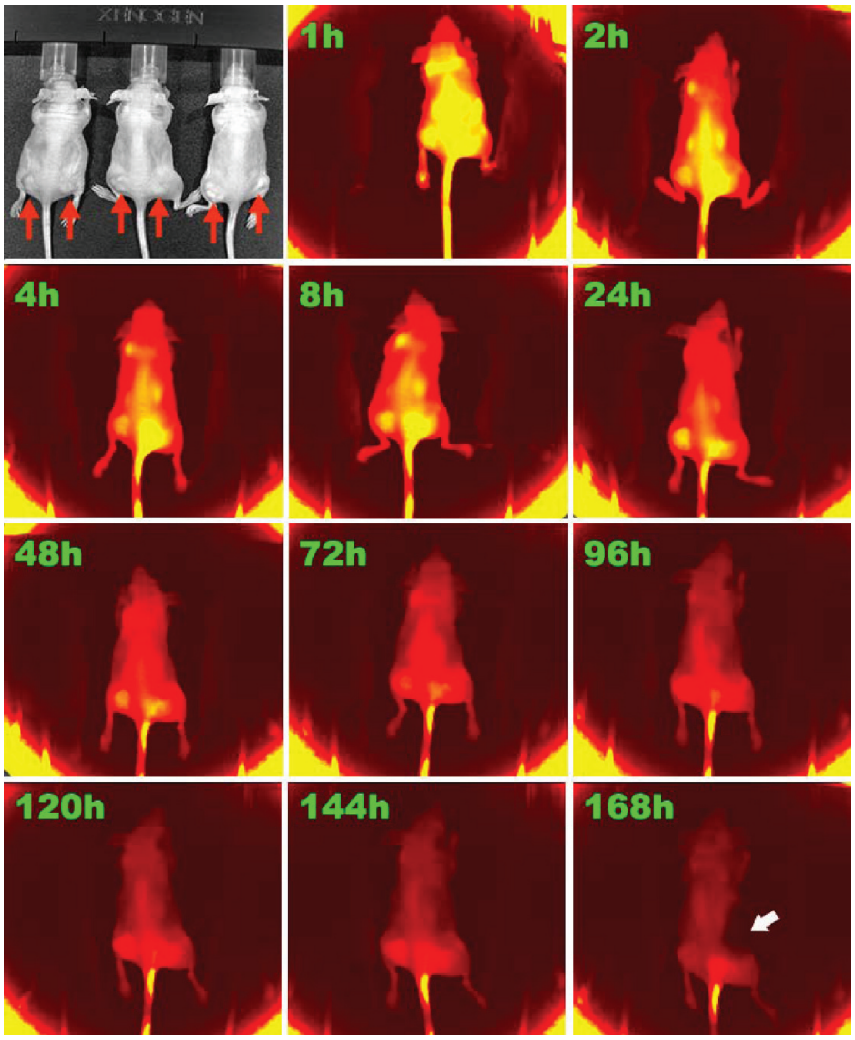

Figure 4. IVIS imaging of MCF-7 tumor-bearing mice. Tumor cells initiated in the flank and marked by red arrows in the bright field image. The fluorescence images were taken at 780 nm (excitation, 740 nm) with the same exposure time (0.25 s), *F*-stop (2), and binning (medium) at different time points after injections. The left mouse was given pure drug nanocrystals; the middle was given hybrid paclitaxel/FPR-749 nanocrystals; the right was given paclitaxel/Rhodamine B nanocrystals. The high intensity rim was due to optical interference by excitation and emission filters. Images were not digitally modified.

certainly due to the dye substance embedded inside nanocrystals. Interestingly, the fluorescence emission of the hybrid nanocrystals visually shifted from green to blue when the dye concentration was reduced. In contrast, the color of pure dye solutions remained unaffected as green. The local hydrophobic environment in the crystal appears to augment the intensity of the dye for fluorescein in particular.

Hybrid nanocrystals were intravenously administered to tumor-bearing mice, and whole-body fluorescence images were taken at various time points (Figure 4). No adverse reactions were observed following tail-vein injection. Mice given the hybrid nanocrystals with FPR-749 clearly showed strong fluorescence at the 780 nm emission wavelength while the two controls (the left and right mice in Figure 4) emitted no significant autofluorescence at that wavelength. Fluorescence intensity at the tumor sites remained observable after 168 h. Interestingly, a high-intensity spot on the tail was also observed, which was likely caused by local accumulation and/or extravascular injection of nanocrystals. Beyond the site of injection, nanocrystals were able to reach the primary tumor site and accumulate. It also appears that, within 4 h, nanocrystals had already reached the tumor sites. Further supporting the notion that the nanocrystals accumulate in the tumor and that the hybrid crystal technology is applicable beyond one fluorophore, Rhodamine B was used as a guest molecule. Unfortunately at 580 nm, there was strong autofluorescence (Figure 5), making the drug/Rhodamine B hybrid nanocrystals difficult to use for the bioimaging purpose. Despite the large background fluorescence, it is apparent that the hybrid nanocrystals had the greatest intensity and that there was apparent (but not quantifiable) accumulation in the tumors.

To further verify the nanocrystal uptake and retention mechanism within tumors, tumor-bearing mice were administered pure FPR-749 solution and compared with animals given paclitaxel/FPR hybrid nanocrystals (Figure 6). When delivered as a solution, the fluorophores (FPR-749) were distributed fairly uniformly and cleared quickly, leaving no significant fluorescence intensity within the tumors after one day. In contrast, high fluorescence intensity was detected when the hybrid nanocrystals were injected. The intensity within the region of the tumor was augmented compared to other tissues. At 24 h, there was

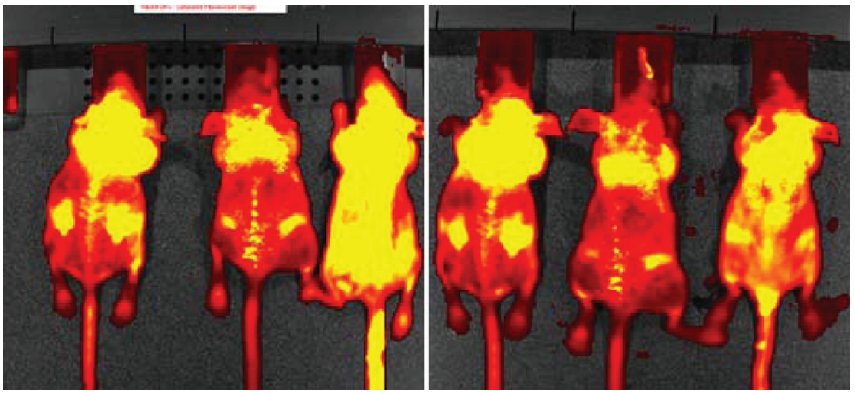

Figure 5. IVIS imaging of the same three mice shown in Figure 4 after receiving the treatment at 1 (left) and 24 h (right). The excitation and emission wavelengths of the fluorescence imaging are 535 and 580 nm, respectively. The left mouse was given pure drug nanocrystals; the middle was given hybrid paclitaxel/FPR-749 nanocrystals; the right was given paclitaxel/Rhodamine B nanocrystals.

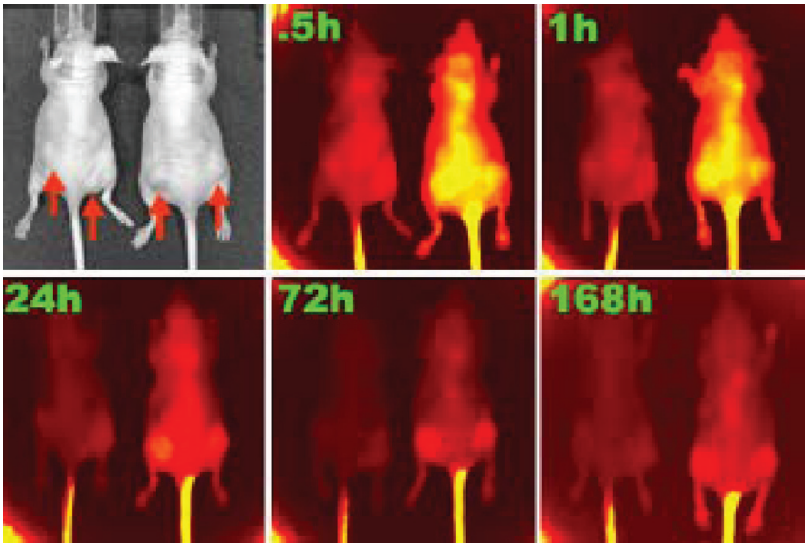

Figure 6. IVIS imaging of two MCF-7 tumor-bearing mice injected with FPR-749 solution (left) and paclitaxel/FPR-749 hybrid nanocrystals (right). Exposure time used was 0.25 s, except for that taken at 168 h (0.5 s).

significantly more intensity in the regions of the tumors which was retained for at least 168 h. Note that the absolute amounts of injected dye molecules were comparable in the two groups. The results suggest that nanocrystals were able to accumulate at the tumor site, supporting the EPR effect being the driving factor for tumor uptake. Also note that the mouse receiving the hybrid nanocrystals showed a large dark spot above the right flank at 168 h (Figure 4, 168 h, arrow): it was actually an injured region due to tumor progression leading to euthanasia. There was local necrosis and gross lack of blood flow in the region. The local injury contained no fluorescent intensity which may be explained by the nanocrystals acting as a depot after accumulating in the tumor. Dye molecules were released from dissolving nanocrystals and returned to the blood circulation. The clearance of free dye molecules was rapid, within 30 min. Thus, the local intensity within the tumor was a result of both released and embedded dyes. Given the dose level of 20 mg/kg used in the study, a mouse of 20 g in weight can have a total concentration of paclitaxel of 200 μg/mL (assuming 2 mL of blood), far exceeding its solubility (ca. 0.2 μg/mL). As such, nanocrystal accumulation in the tumor is expected to be due to the enhanced permeability and retention effect (EPR).

The size of the nanocrystals is on the larger end of the fenestration width reported for tumors; however, the high aspect ratio and initial dissolution upon injection may allow the particles to fit through the fenestration which are typically reported to be between 100 and 500 nm. Moreover, the subcutaneous tumors may facilitate the extravasation of the hybrid nanocrystals because of the range of pore size of tumor vasculature, which may reach up to 1.2 μm in mice.[15] The accumulation through this effect is further supported by the fact that nanocrystals were retained within the tumor mass for several days while the fluorescent dye, injected alone, was rapidly cleared from the mice. The fluorescence in the vicinity of the tumor is retained for a substantial time, suggesting slow dissolution within the tumor. Further confirmation of the presence of nanocrystals within the tumor is necessary to validate this, but the retention of fluorescence is suggestive of nanocrystal retention since the pharmacokinetic elimination of the free small molecules was rapid.

After the end point, the tumors and major organs were harvested and imaged (Figure 7). The tumors showed strong FPR-749 fluorescence, followed by kidney, lung, and much weaker fluorescence in liver; heart, spleen, and brain showed little detectable fluorescent

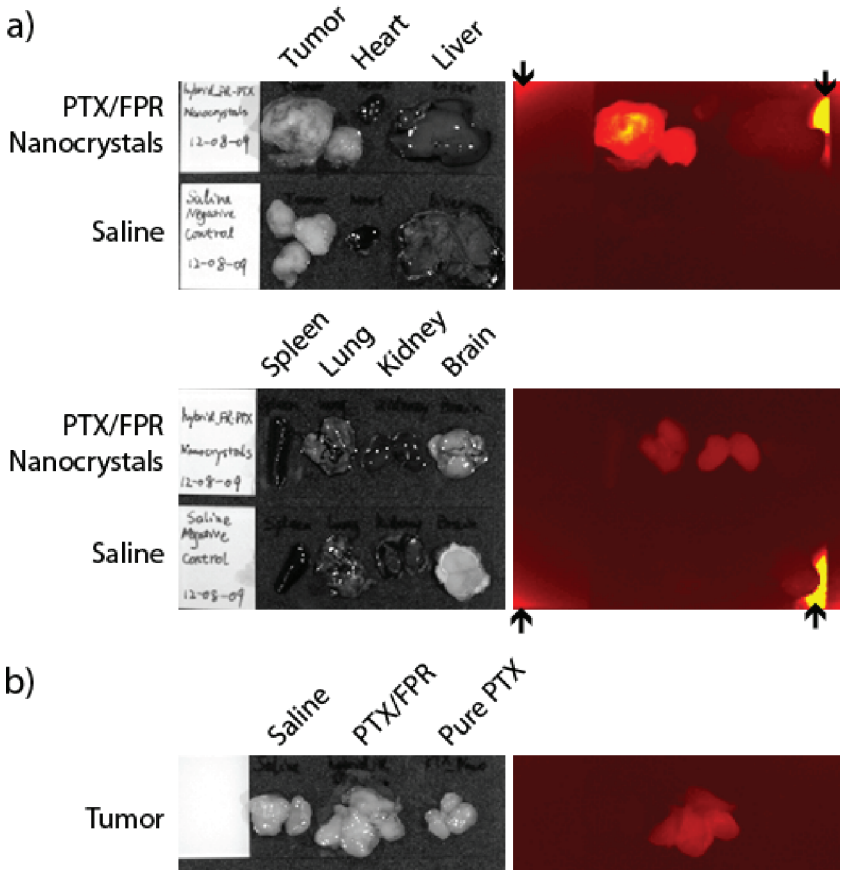

Figure 7. Postmortem tumor and tissue samples of tumor-bearing mice treated with paclitaxel (PTX) pure and dye hybrid nanocrystals, as well as negative control, saline. The black-and-white (left) and fluorescent (right) photos were taken by IVIS. The settings of the fluorescent imaging were identical to those used in Figure 4, except for exposure (0.5 s); the bright rim (marked by arrows) was due to optical artifacts. (a) Comparison of tumors and major organs treated between hybrid nanocrystals and saline. (b) Comparison of tumors treated differently.

intensity. The relatively large uptake in kidney and lung was possibly explained by filtration and clearance of the nanocrystals from the blood by immune cells of the reticuloendothelial system (RES), as commonly observed in delivering nanomedicines. It is also possible that aggregation of particles occurred in the physiologic fluids due to charge shielding effect of the ions. We hope to investigate this possibility in the near future, and this is one reason that we injected intravenously from distilled water to minimize potential aggregation upon injection. Once the aggregation phenomena are understood, we will inject from more physiologically acceptable fluids. However, we do not feel that the possible aggregation of the particles upon injection would allow local accumulation in the tumors. The lung, kidney and injection site accumulation may be explained, at least in part, by the aggregation of the particles, but large particles would not be expected to enter through the tumor's fenestrated endothelium from the blood. Moreover, the antitumor effect by the pure and hybrid nanocrystals is expected, as demonstrated by our recent study of camptothecin nanocrystals,[16] and the results of tumor reduction are being analyzed and will be published soon.

CONCLUSION

Antitumor effect was observed by using pure and hybrid nanocrystals and results being collected. The bioimaging results here support the clinical potential of using hybrid nanocrystals to treat solid tumors and, at the same time, to track the drug particles in real time. The novelty of our concept lies in physically integrating imaging molecules inside the crystal lattice of drug nanocrystals to be delivered. No chemical conjugation is required, and functional guest substances distribute throughout the hosting drug solid particles.

AUTHOR INFORMATION

Corresponding Author

*375 Biopharm Complex, 789 South Limestone Street, Lexington, KY 40536. Tel: +1(859) 257-1472. Fax: (859)257-7585. E-mail: tonglei@uky.edu.

ACKNOWLEDGMENT

This work was supported by DOD Breast Cancer Research Program (BC050287). The authors would like to thank University of Kentucky Department of Toxicology for allowing us to use the IVIS system.

REFERENCES

(1) Allen, T. M.; Cullis, P. R. Drug delivery systems: Entering the mainstream. *Science* **2004**, *303* (5665), 1818–1822.

(2) Peer, D.; Karp, J. M.; Hong, S.; FaroKhzad, O. C.; Margalit, R.; Langer, R. Nanocarriers as an emerging platform for cancer therapy. *Nat. Nanotechnol.* **2007**, *2* (12), 751–760.

(3) Maeda, H.; Wu, J.; Sawa, T.; Matsumura, Y.; Hori, K. Tumor vascular permeability and the EPR effect in macromolecular therapeutics: A review. *J. Controlled Release* **2000**, *65* (1−2), 271–284.

(4) Baba, K.; Pudavar, H. E.; Roy, I.; Ohulchanskyy, T. Y.; Chen, Y. H.; Pandey, R. K.; Prasad, P. N. New method for delivering a hydrophobic drug for photodynamic therapy using pure nanocrystal form of the drug. *Mol. Pharmaceutics* **2007**, *4* (2), 289–297.

(5) Merisko-Liversidge, E.; Sarpotdar, P.; Bruno, J.; Hajj, S.; Wei, L.; Peltier, N.; Rake, J.; Shaw, J. M.; Pugh, S.; Polin, L.; Jones, J.; Corbett, T.; Cooper, E.; Liversidge, G. G. Formulation and antitumor activity evaluation of nanocrystalline suspensions of poorly soluble anticancer drugs. *Pharm. Res.* **1996**, *13* (2), 272–278.

(6) Rabinow, B.; Kipp, J.; Papadopoulos, P.; Wong, J.; Glosson, J.; Gass, J.; Sun, C. S.; Wielgos, T.; White, R.; Cook, C.; Barker, K.; Wood, K. Itraconazole IV nanosuspension enhances efficacy through altered pharmacokinetics in the rat. *Int. J. Pharm.* **2007**, *339* (1−2), 251–260.

(7) Junghanns, J.; Muller, R. H. Nanocrystal technology, drug delivery and clinical applications. *Int. J. Nanomed.* **2008**, *3* (3), 295–309.

(8) Rabinow, B. E. Nanosuspensions in drug delivery. *Nat. Rev. Drug Discovery* **2004**, *3* (9), 785–796.

(9) Horn, D.; Rieger, J. Organic nanoparticles in the aqueous phase - theory, experiment, and use. *Angew. Chem., Int. Ed.* **2001**, *40* (23), 4331–4361.

(10) Muller, R. H.; Keck, C. M. Challenges and solutions for the delivery of biotech drugs - a review of drug nanocrystal technology and lipid nanoparticles. *J. Biotechnol.* **2004**, *113* (1−3), 151–170.

(11) Kahr, B.; Gurney, R. W. Dyeing crystals. *Chem. Rev.* **2001**, *101* (4), 893–951.

(12) Hermus, L.; van Dam, G. M.; Zeebregts, C. J. Advanced carotid plaque imaging. *Eur. J. Vasc. Endovas. Surg.* **2010**, *39* (2), 125–133.

(13) Kim, D. E.; Kim, J. Y.; Schellingerhout, D.; Kim, E. J.; Kim, H. K.; Lee, S.; Kim, K.; Kwon, I. C.; Shon, S. M.; Jeong, S. W.; Im, S. H.; Lee, D. K.; Lee, M. M.; Kim, G. E. Protease imaging of human atheromata captures molecular information of atherosclerosis, complementing anatomic imaging. *Arterioscler., Thromb., Vasc. Biol.* **2010**, *30* (3), 449–U186.

(14) Liggins, R. T.; Hunter, W. L.; Burt, H. M. Solid-state characterization of paclitaxel. *J. Pharm. Sci.* **1997**, *86* (12), 1458–1463.

(15) Hobbs, S. K.; Monsky, W. L.; Yuan, F.; Roberts, W. G.; Griffith, L.; Torchilin, V. P.; Jain, R. K. Regulation of transport pathways in tumor vessels: Role of tumor type and microenvironment. *Proc. Natl. Acad. Sci. U.S.A.* **1998**, *95* (8), 4607–4612.

(16) Zhang, H.; Hollis, C. P.; Zhang, Q.; Li, T. Preparation and antitumor study of camptothecin nanocrystals. *Int. J. Pharm.* **2011**, *415*, 293–300.